JACS
JOURNAL OF THE AMERICAN CHEMICAL SOCIETY
pubs.acs.org/JACS
Article

High-Spin [Fe^{I}_3] Cluster Capable of Pnictogen Atom Capture

Trevor P. Latendresse, Nicholas P. Litak, Joy S. Zeng, Shao-Liang Zheng, and Theodore A. Betley*

Cite This: J. Am. Chem. Soc. 2024, 146, 25578−25588
Read Online
ACCESS | Metrics & More | Article Recommendations | Supporting Information

ABSTRACT: Using a new hexanucleating anildophosphine ligand $^{tBu}LH_3$ (1,3,5-C_6H_9(NHC_6H_3−5-F−2-$P(tBu)_2$)$_3$), the all-monovalent [Fe^{I}_3] compound (^{tBu}L)Fe_3 (**1**) was isolated and characterized by X-ray diffraction analysis, SQUID magnetometry, ^{57}Fe Mössbauer spectroscopy, and cyclic voltammetry. The molecular structure of **1** reveals very close Fe−Fe distances of 2.3825(7), 2.4146(8), and 2.3913(8) Å which results in significant Fe−Fe interactions and a maximum high-spin $S = {}^{9}/_{2}$ spin state as determined by SQUID magnetometry and further supported by quantum chemical calculations. Compound **1** mediates the multielectron, oxidative atom transfer from inorganic azide ([Bu_4N][N_3]), cyanate (Na[NCO]), and phosphonate (Na-(dioxane)$_{2.5}$[PCO]) to afford the [Fe_3]-nitrido (N^{3-}) and [Fe_3]-phosphido (P^{3-}) pnictides, (^{tBu}L)Fe_3(μ^3−N) (**2**) and [(^{tBu}L)Fe_3(μ^3−P)(CO)]$^-$ (**3**), respectively. Compounds **1**−**3** exhibit rich electrochemical behavior with three (for **1**), four (for **2**) and five (for **3**) distinct redox events being observed in the cyclic voltammograms of these compounds. Finally, the all−monovalent **1** and the formally $Fe^{II}/Fe^{II}/Fe^{I}$ compound **3**, were investigated by alternating current (ac) SQUID magnetometry, revealing slow magnetic relaxation in both compounds, with **3** being found to be a unique example of a [Fe_3]-phosphido single-molecule magnet having an energy barrier relaxation reversal of $U = 30.7(6)$ cm^{-1} in the absence of an external magnetic field. This study demonstrates the utility of an all low-valent polynuclear cluster to perform multielectron redox chemistry and exemplifies the redox flexibility and unique physical properties that are present in the corresponding midvalent oxidation products.

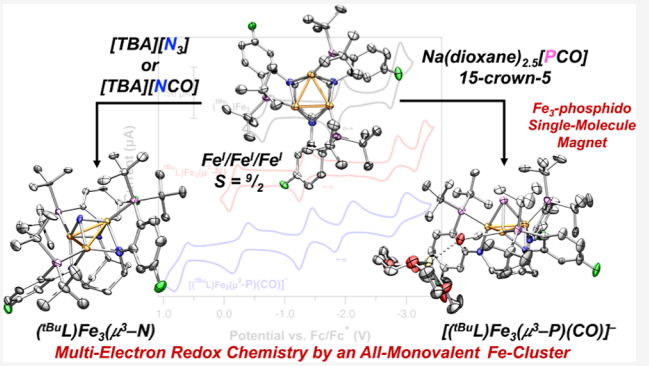

1. INTRODUCTION

The design of molecular systems that can catalyze the reduction of small molecule substrates into their more desirable constituents have important implications in areas such as N_2 fixation[1−3] and CO/CO_2 reduction.[4−6] Full reductive conversion of each of the substrates mentioned constitutes a multielectron process. In nature, multielectron reduction chemistry is often performed at multinuclear cluster cofactors which have been preloaded with reducing equivalents prior to substrate uptake.[7−9] Likewise, many industrial processes use heterogeneous catalysts composed of electron rich, nominally zerovalent, transition metal sites to achieve multielectron reduction of substrates.[10] Inspired by both biological and industrial processes, chemists have sought to perform multielectron reductive chemistry using compounds featuring highly reducing/electron rich low-valent transition metals such as $Fe^{I/0}$ and $Co^{I/0}$.[11−28] Indeed, low-valent transition metal compounds have been shown to mediate multielectron reductive transformations of environmentally/biologically relevant small molecules such as N_2,[1−3,11−16] CO_2,[29−31] and CO.[32−34] To this end, the development of molecular systems that can perform multielectron reductive transformations at efficiencies rivaling heterogeneous/biological processes is an ongoing challenge.

Previously reported low-valent molecular systems typically propose an intermolecular redox mechanism between two or more clusters to achieve the complete reduction of substrate. For example, Walter[12] and Holland[16] have shown that reduction of [(L)Fe^{II}(X)]$_2$ (L = cyclopentadienide or β-diketiminate) halide dimers in the presence of N_2 results in the formation of polymetallic bis-nitrido products of the type, {((L)Fe)$_{3-4}$(N^{3-})$_2$}, indicating that three or more [(L)Fe^{I}] fragments are involved in the full reduction of dinitrogen. This precedent contrasts the proposed mechanism of many industrial and biological small molecule reduction processes,[8−10] where electron transfer to substrate is proposed to occur at a single polynuclear active site stationed within a protein or heterogeneous catalyst surface, respectively. In this light, low-valent molecular clusters that can perform concerted multielectron reductions on a cooperatively bound substrate

Received: May 24, 2024
Revised: August 13, 2024
Accepted: August 14, 2024
Published: September 4, 2024

https://doi.org/10.1021/jacs.4c07112
J. Am. Chem. Soc. 2024, 146, 25578−25588

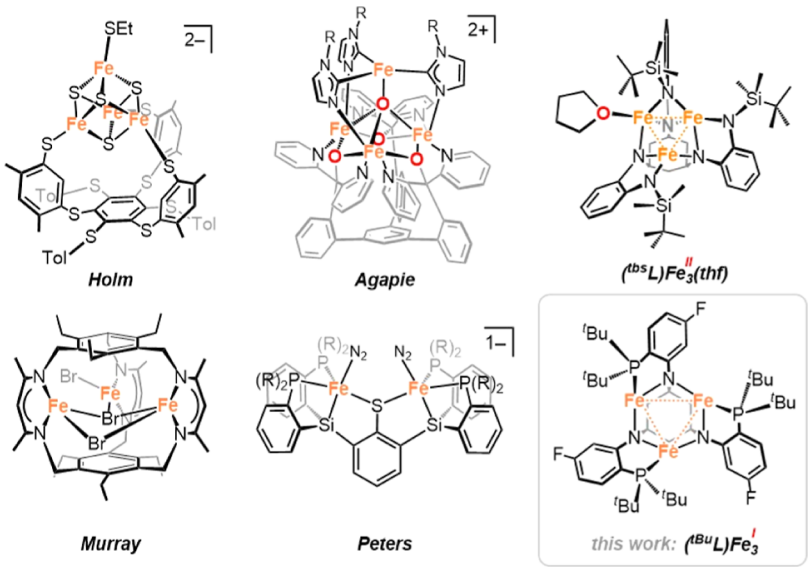

Figure 1. Selected examples of well-defined ligand templated Fe clusters[13,40,41,44,45] and the trinuclear [Fe^{I}_3] cluster presented in this work.

Scheme 1. Synthesis of the Trinucleating Anildophosphine Proligand $^{tBu}LH_3$

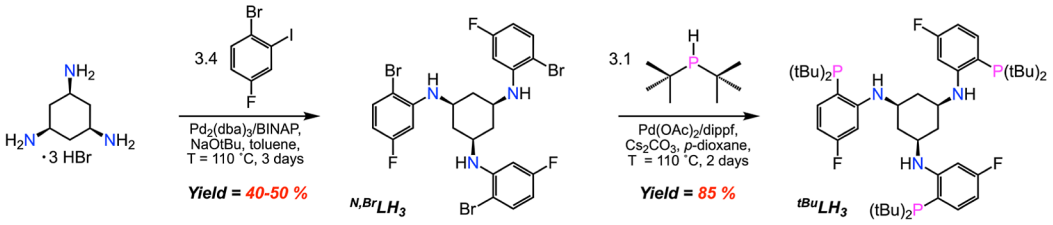

could lead to reduction chemistry more akin to biological/industrial processes.

We and others have used polynucleating ligand scaffolds to proximally coordinate multiple transition metals within a single molecule for the purpose of achieving cooperative substrate uptake capable of mediating multielectron redox chemistry (Figure 1).[35−44] This strategy has resulted in molecular clusters having expanded redox capacities for a single molecule and structurally dynamic metal cores that can stabilize the highly reactive intermediates involved in multielectron transformations. The vast majority of reported templating ligands for polynuclear transition metal clusters are designed to stabilize mid- to high-valent metals, where the average formal oxidation state of the cooperating metal ions is +2 or higher. Ligand-templated clusters containing only low-valent transition metal centers have been largely underexplored. Two notable exceptions are a binucleating phosphinothiolate-based scaffold reported by Peters which stabilizes two Fe^{I} ions[41] and a trinucleating β-diketiminate-based scaffold reported by Murray which supports a putative [$Fe^{I}]_3$ cluster in route to N_2 reduction to form the all-ferric poly imido species, (L)-$Fe_3(NH)_3$.[13] For the later, substrate reduction is proposed to proceed through an intermolecular mechanism despite the availability of a polynulcear Fe^{I} core. This assertion is made based on the Fe/N ratio of the higher valent Fe-imido reaction products along with the cocrystallization of a dimeric {(L)Fe_3-N_x}$_2$ species akin to reaction products obtained from the mononuclear analogues.[16]

Our group has previously shown that the tris-*o*-phenylenedianilide ligand scaffold [^{tbs}L]$^{6-}$ can be used to isolate the all-ferrous cluster (^{tbs}L)Fe_3(thf) which features three strongly interacting Fe^{2+} centers resulting in a maximally high-spin (S = 6) [Fe^{II}_3] core.[45] The strongly correlated polynuclear core of (^{tbs}L)Fe_3(thf) facilitates multielectron oxidative group transfer chemistry of nitrogenous-based reagents such as inorganic/organic azides and hydrazines to form the corresponding bridging Fe_3-imido or Fe_3-nitrido species.[46] Though the [^{tbs}L]$^{6-}$ scaffold allows access to a breadth oxidative chemistry at the [Fe^{II}_3] core of (^{tbs}L)Fe_3(thf), the hexa-anionic ligand scaffold has thus far not been found suitable for isolating all-low valent [Fe_3^{n+}] (n < +2) systems, likely due to the very low reduction potentials and/or charge accumulation such a system would incur. To gain access to all low-valent [Fe^{I}_3] clusters, we sought to modify the hexa-anilide ligand platform through replacement of the three peripheral anilides with tertiary phosphines. The increased σ-donating [and potentially π-accepting (for $P(Ar)_3$ or $P(OAr)_3$)][47] capabilities of tertiary phosphines along with trianionic nature of the proposed tris-anilidophosphine ligand ([^{tBu}L]$^{3-}$) could potentially stabilize all-monovalent clusters of the type (L)Fe^{I}_3 as neutral species.

Herein, we report the synthesis of a new polynucleating tris-anilidophosphine ligand ([^{tBu}L]$^{3-}$) and its use in isolating an all Fe^{I} cluster (^{tBu}L)Fe_3 (**1**) which features a maximally high spin $S = {}^{9}/_{2}$ [Fe^{I}_3] core. Compound **1** facilitates intramolecular multielectron reduction of inorganic/organic azides, cyanates, and phosphonates to give the corresponding [Fe_3]-pnictides (^{tBu}L)$Fe_3(\mu^3$−N) (**2**) and [(^{tBu}L)$Fe_3(\mu^3$−P)(CO)]$^-$ (**3**), respectively, where mixed-valent **3** represents a rare example of a paramagnetic transition metal complex featuring a bridging phosphido ligand. The nitrido and phosphido adducts **2** and **3**, respectively, exhibit rich electrochemistry with at least four redox events being observed for each compound. Furthermore,

https://doi.org/10.1021/jacs.4c07112
J. Am. Chem. Soc. 2024, 146, 25578−25588

investigation of the low-valent compounds **1** and **3** by SQUID magnetometry suggests that slow magnetic relaxation is apparent in both compounds, with compound **3** exhibiting single-molecule magnetic behavior in the absence of an external magnetic field. This study illustrates a unique example of intramolecular, multielectron, redox chemistry by an all low-valent triiron complex and showcases the rich redox chemistry latent in the midvalent oxidation products.

2. RESULTS AND DISCUSSION

2.1. Synthesis of $^{tBu}LH_3$. To aid the characterization of potentially paramagnetic low-valent clusters, we sought to incorporate fluorine into the ligand backbone of the targeted $[^{tBu}L]^{3-}$ scaffold to be used for in situ reaction monitoring by ^{19}F NMR. The fluorinated, tris-anilidophosphine ligand $^{tBu}LH_3$ can be synthesized in two steps using consecutive Pd-catalyzed reactions as shown in Scheme 1. Trifold arylation of 1,3,5-triaminocyclohexane hydrobromic acid with three equivalents of 1,2,4-bromo-iodo-fluorobenzene ($Pd_2(dba)_3$/BINAP, toluene, 120 °C for 3 days) affords the tribromo-triaryl precursor $^{N,Br}LH_3$ in 40−50% isolated yields on a multigram scale. Subsequent derivatization of $^{N,Br}LH_3$ is achieved through a subsequent cross-coupling reaction of $^{N,Br}LH_3$ with 3.1 equiv of tBu_2PH ($Pd(OAc)_2$/1,1′-diisopropylferrocene (dippf), *p*-dioxane, 110 °C for 2 days) to afford the desired anilidophosphine pro-ligand $^{tBu}LH_3$ in 85% yield after filtration of the reaction mixture through a silica plug and evaporation of the filtrate volatiles. The composition of $^{tBu}LH_3$ was confirmed by high-resolution mass-spectroscopy ($[M + H^+]$ m/z = 844.5200) and multinuclear NMR spectroscopy where a single resonance was observed in the ^{19}F NMR (−109.72 ppm) and ^{31}P (−0.54 ppm) NMR spectra, thus confirming the C_3-symmetry of $^{tBu}LH_3$ in solution.

2.2. Synthesis and Characterization of $(^{tBu}L)Fe_3$. Transamination of $^{tBu}LH_3$ with previously prepared Fe^{I} synthons $(L)Fe(N(SiMe_3)_2)$[48] or the anionic bis-amido analogue, $[Fe(N(SiMe_3)_2)_2]^{-}$[49] was unsuccessful. Thus, we targeted the all-Fe^{I} containing cluster by initial metalation of $[^{tBu}L]^{3-}$ with three equivalents of a suitable ferrous salt followed by a trifold chemical reduction (Figure 2a). The putative all ferrous precursor (e.g., $(^{tBu}L)Fe_3Br_3$) was synthesized by deprotonation of $^{tBu}LH_3$ with three equivalents of *n*-butyllithium and the subsequent addition of 3.05 equiv of $FeBr_2$ at room temperature. The resulting dark red solution was stirred at room temperature for 1.5 h and was then heated for an additional 1.5 h to ensure 3-fold metalation as monitored by ^{19}F NMR. Three broad resonances of −36, −39, and −55 ppm in the ^{19}F NMR spectrum suggests a non-C_3 symmetric Fe^{II}-metalated product in THF solution (Figure S10).

Chemical reduction of the putative $(^{tBu}L)Fe_3Br_3$ was accessed by the addition of 3.1 equiv of KC_8 to a thawing solution of the metalated ligand. Upon KC_8 addition, the three ^{19}F NMR resonances of the kinetic metalation product coalesce into a single, upfield shifted, resonance (−68 ppm), indicative of C_3 symmetry of the tris-anilidophosphine ligand scaffold (Figure S12). Indeed, the formation of the all-Fe^{I} cluster $(^{tBu}L)Fe_3$ (**1**) was confirmed via high-resolution mass spectrometry ($[M + H^+]$ m/z = 1009.3028) and can be isolated as a pure black solid (yield = 48%) following extraction from the solid reaction mixture with hexanes and removal of the volatiles.

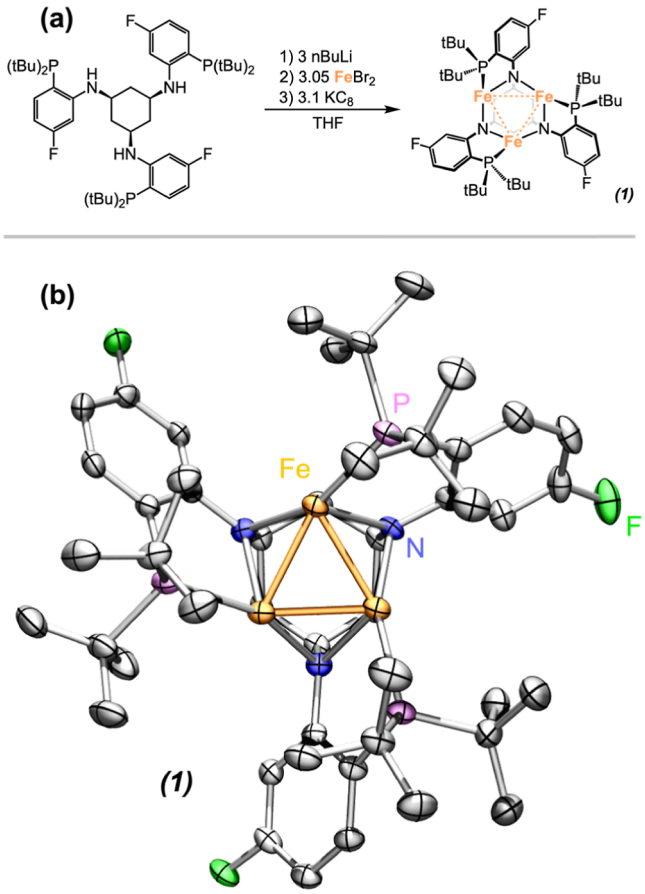

Figure 2. (a) Synthesis of the putative $(^{tBu}L)Fe_3Br_3$ and subsequent reduction to generate $(^{tBu}L)Fe_3$ (**1**). (b) Molecular structure of **1**. Atom colors represent Fe (orange), N (blue), P (pink), F (green), C (gray). H atoms omitted for clarity. Structure presented with ellipsoids at 50% probability.

Crystals of **1** suitable for analysis by single-crystal X-ray diffraction (SCXRD) were afforded by recrystallization out of concentrated hexanes/benzene (~20:1) solutions at −35 °C for 1−2 days. The molecular structure of **1** features a trinuclear $[Fe_3]$ core supported by a nearly ideal C_3-symmetric $[^{tBu}L]^{3-}$ ligand framework (Fe−P (Å): 2.2976(12), 2.3136(11), 2.2895(11); Fe−N (Å): 2.037(3), 2.087(3), 2.050(3), 2.093(3), 2.036(3), 2.088(3); Fe−Fe (Å): 2.3825(7), 2.4146(8), 2.3913(8)) (Figure 2b). Neglecting Fe−Fe interactions, each Fe site adopts a distorted T-shaped geometry consisting of two bridging anilido ligands and a periphery di-*tert*-butyl phosphine ligand. Despite the slight deviation from ideal C_3symmetry that is observed in the solid-state structure of **1**, the solid state ^{57}Fe Mössbauer spectrum of **1** exhibits a single resolved quadrupole doublet (δ, $|\Delta E_Q|$ (mm/s): 0.62, 2.38), indicating only very small differences in the electric-field gradient around the individual Fe sites (Figure S46). The Fe−Fe distances of **1** of 2.3825(7), 2.4146(8), and 2.3913(8) Å are well within the range of the sum of the covalent radii of two Fe atoms (3.04 Å)[50] and indicate non-negligible Fe−Fe bonding interactions within the $[Fe_3]$ core of **1**. Notably, the average Fe−Fe distance of **1** (2.3961[4] Å) is shorter than the corresponding average distance of $(^{tbs}L)Fe_3(thf)$ (2.5769[2] Å),[45] and the singly reduced, $[(^{tbs}L)Fe_3]^{-}$ (2.4459[8] Å)[51] but is slightly longer than the average Fe−Fe distance of the all ferrous cluster $(^{H}L)Fe_3(PMe_3)_3$ (2.299[19] Å) which is

https://doi.org/10.1021/jacs.4c07112
J. Am. Chem. Soc. 2024, 146, 25578−25588

templated by a related hexanionic polyanilide ligand and three exogenous trimethylphosphine ligands (Table 1).[43]

Table 1. Comparison of Fe−Fe Distances and Spin-State of Compounds of Selected [Fe_3] Compounds

compound	avg. Fe−Fe distance (Å)	formal $Fe^{n+}/Fe^{n+}/Fe^{n+}$ ox. state	{Fe_3} $3d^n$ count	S
(^{tbs}L)Fe_3(thf)	2.5769[2]	2+/2+/2+	$3d^{18}$	6
[(^{tbs}L)Fe_3]$^-$	2.4459[8]	1+/2+/2+	$3d^{19}$	$^{11}/_2$
(^{H}L)$Fe_3(PMe_3)_3$	2.299[19]	2+/2+/2+	$3d^{18}$	1
(^{tBu}L)Fe_3 (**1**)	2.3961[8]	1+/1+/1+	$3d^{21}$	$^{9}/_2$

We have previously shown that for (^{tbs}L)Fe_3(thf) and [(^{tbs}L)Fe_3]$^-$ the close Fe−Fe contacts in combination with the weak ligand field results in a maximum spin state for high spin $3d^{18}$ (S = 6) and $3d^{19}$ (S = $^{11}/_2$) [Fe_3] cores, respectively. In contrast, the trimethylphosphine bound cluster (^{H}L)-$Fe_3(PMe_3)_3$ which has the shortest Fe−Fe distances of the series (2.299[19] Å), adopts an S = 1 ground configuration that is expected for a low spin $3d^{18}$ [Fe_3] core.[43] Given the intermediate Fe−Fe distance of **1** and the mixture of strong and weak field ligand donor atoms of the supporting [^{tBu}L]$^{3-}$ scaffold, we were interested in exploring the electronic structure of **1** via SQUID magnetometry. The static magnetic properties of **1** were investigated by measuring the direct current (dc) magnetic susceptibility under a 1 T external magnetic field and cooling from T = 300−2 K (Figure 3). The

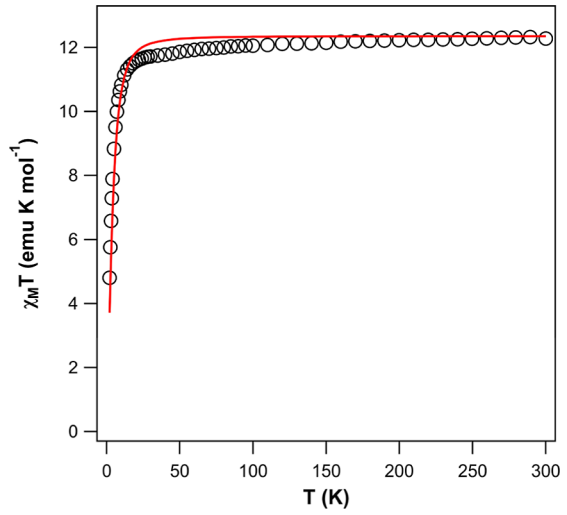

Figure 3. Temperature dependence of the molar magnetic susceptibility temperature product ($\chi_M T$) of **1** (T = 300−2 K; H = 1 T). Line represents fit to experimental data (open circles). (S = 9/2, g = 2.00, D = −2.2 cm^{-1}, and E = 0.70 cm^{-1} (|E/D| = 0.32)).

$\chi_M T$ (300 K) value of 12.28 emu·K mol^{-1} for **1** is very close to the expected value of 12.375 emu·K mol^{-1} for a system with an S = $^{9}/_2$ ground state and is consistent with a maximally high-spin [Fe^{I}_3] trinuclear core. Upon cooling, the $\chi_M T$ value remains nearly constant until 16 K, where a steep decline is observed to a minimum value of 4.80 emu·K mol^{-1} at 2 K. Such low temperature declines in the $\chi_M T$ vs T plots are often attributed non-negligible zero-field splitting (ZFS) or population of a lower spin electronic ground state. To further investigate the spin-ground state of **1**, variable temperature magnetization data was collected for compound **1** between 2 and 8 K (Figure S33). At 2 K, the magnetization reaches a maximum value of 6.90 μ_B at the 7 T instrument field limit. The experimentally observed magnetic saturation value is lower than the expected value of 9 μ_B for an ideal S = $^{9}/_2$ (g = 2) spin system. This observation indicates the non-negligible ZFS and is further confirmed by the nonsuperposition of the reduced magnetization (M vs H/T) curves (Figure S34). The susceptibility and magnetization data for **1** were simultaneously fit using a giant spin Hamiltonian[52]

$$\hat{H} = D\hat{S}_z^2 + E(\hat{S}_x^2 - \hat{S}_y^2) + g_{iso}\mu_B S\cdot H \quad (1)$$

Assuming a S = $^{9}/_2$ ground state, reasonable fits were obtained giving best fit parameters of g = 2.00, D = −2.2 cm^{-1}, and E = 0.70 cm^{-1} (|E/D| = 0.32).

2.3. Computational Analysis of 1. We next sought to describe the electronic structure of **1** and a qualitative molecular orbital diagram for **1** was constructed from first-principles ligand field theory (Figure 4). As described above,

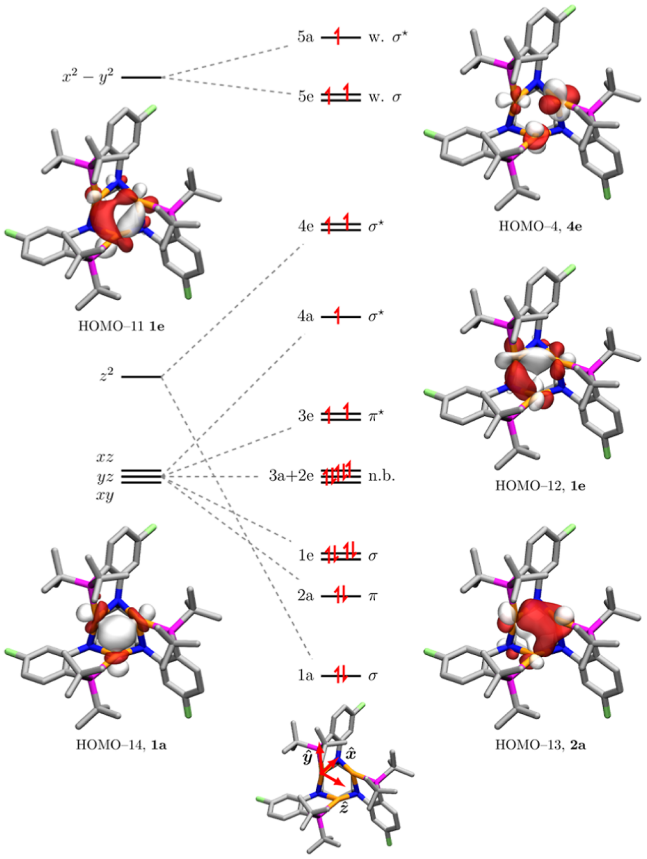

Figure 4. Qualitative MO diagram and selected quasi-restricted orbital output of **1**.

each iron center sits in a distorted T-shaped geometry with a phosphine and bridging anilido donor at the arm of the T and the second bridging anilido at the stem. These ligand donors define the x and y axes, positioning the z axis toward the centroid above [Fe_3] core. The initial d_{xz} and d_{yz} orbitals arising from this choice of coordinates were allowed to mix such that the new d_{xz} and d_{yz} orbitals are oriented parallel and orthogonal to the [Fe_3] core, respectively. The primary Fe−Fe σ-bonding interaction are derived from the d_{z2} and d_{xz} orbitals, and the d_{yz} orbitals provide π-bonding across the trinuclear

https://doi.org/10.1021/jacs.4c07112
J. Am. Chem. Soc. 2024, 146, 25578−25588

core (see the Supporting Information for the full bonding scheme).

DFT calculations were performed using the ORCA 5.0.4[53] package to corroborate our bonding model. A full description of the calculation methods employed can be found in the Supporting Information. First, geometry optimization calculations were performed starting from the solid-state structure of ($^{t\mathrm{Bu}}$L)Fe$_3$ using a variety of functionals and calculation procedures. All calculated structures reproduced the pseudo-C_3 symmetry of the [Fe$_3$] core, but the optimized structure **1**$^{\mathrm{opt}}$ that was obtained using the TPSSh[54,55] functional with the zeroth-order regular approximation and Ahlrichs def2 basis set (Fe: ZORA-def2-TZVP, rest: ZORA-def2-SVP)[56,57] best replicated the Fe−Fe bonding within the core of **1**. Additionally, a rigorously C_3 symmetric cluster (**1′**) with the inter-Fe distance set to the average Fe−Fe distance of **1** (2.397 Å) was generated using a simple Python script and was also used for single point calculations. Both **1**$^{\mathrm{opt}}$ and **1′** very closely capture all the bond metrics in the solid-state structure of **1**.

Single point calculations were performed on **1**$^{\mathrm{opt}}$ and **1′** using the same procedure as the geometry optimization of **1**$^{\mathrm{opt}}$ except the Ahlrichs basis set of triple-ζ valence quality was used for all atoms. The canonical orbitals exhibited considerable delocalization and mixing among the Fe d-orbitals that were minimized in the quasi-restricted orbitals (QRO) in which we could identify 15 isolated metal-based orbitals. The QRO outputs from **1**$^{\mathrm{opt}}$ and **1′** were qualitatively identical, but less mixing was observed with the rigorously C_3-symmetric structure. Overall, the calculated electronic structure supports our proposed molecular orbital diagram (Figure 4). The lowest energy metal-based orbital is the d_{z^2} all in-phase combination (approximate *a* symmetry) which is followed by all in-phase combination of d_{yz} and the doubly degenerate set of d_{xz} (of approximate *e* symmetry). The HOMO and next two lowest energy molecular orbitals are clear $d_{x^2-y^2}$ orbitals. Doubly degenerate antibonding orbitals arising from the d_{z^2} are also found in the QRO output as well as two of the nonbonding d_{xy} orbitals. The remaining five orbitals exhibit considerable mixing that makes assignment of their parentage difficult.

Finally, a spin state analysis was performed on **1**$^{\mathrm{opt}}$ in which single-point calculations were carried out at spin states ranging from high ($S = {}^9/_2$) to low spin ($S = {}^1/_2$). The $S = {}^9/_2$ state was calculated to be lowest in energy, and it is stabilized by 12.5 kcal/mol relative to the next lowest energy spin state ($S = {}^7/_2$) which corroborates the experimentally observed ground state of **1** suggested by SQUID magnetometry.

2.4. Redox Chemistry of Compound 1: Pnictogen Atom Capture. We were interested in the capacity of **1** to effect inner-sphere redox transformation concomitant with small molecule activation processes. Addition of a THF solution of tetrabutylammonium azide (1 equiv) to a frozen slurry of **1** resulted in a color change of the reaction solution from black to dark red upon warming from frozen THF solution to room temperature. After 20 min, complete conversion of **1** to a new C_3-symmetric product was observed as suggested by a single, upfield ^{19}F NMR resonance at −109 ppm (Figure S15). Correspondingly, the ^{1}H NMR spectrum shows a set of 8 new resonances close to the diamagnetic region between 13 and −4 ppm (Figure S14).

The apparent diamagnetism of the new C_3 symmetric product was further supported by the observation of a sharp ^{31}P NMR resonance at −24 ppm (Figure S17) which is notably shifted upfield from the −0.54 ppm ^{31}P resonance of free ligand $^{t\mathrm{Bu}}$LH$_3$. Crystallization of the crude reaction mixture out of cold pentane resulted in black single crystals which were determined to be the neutral Fe$_3$-nitrido species ($^{t\mathrm{Bu}}$L)Fe$_3$(μ^3−N) (**2**) by SCXRD (Figure 5).

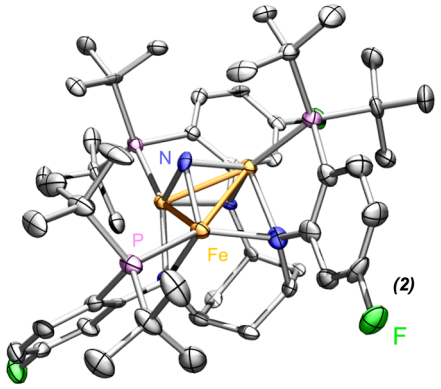

Figure 5. Molecular structure of **2**. Atom colors represent Fe (orange), N (blue), P (pink), F (green), C (gray). H atoms omitted for clarity. Structure presented with ellipsoids at 50% probability.

Compound **2** has a formal Fe$^{\mathrm{II}}$/Fe$^{\mathrm{II}}$/Fe$^{\mathrm{II}}$ core and suggests a three-electron oxidation of **1** upon azide addition. One possible mechanism for the formation of all ferrous **2** is the disproportionation of an Fe$^{\mathrm{II}}$/Fe$^{\mathrm{II}}$/Fe$^{\mathrm{I}}$ [($^{t\mathrm{Bu}}$L)Fe$_3$(μ^3−N)]$^-$ intermediate into neutral **2** and other reduced species. Although the reduction product(s) have not been identified crystallographically, this mechanism is supported by the ^{57}Fe Mössbauer spectrum of the crude reaction mixture after the addition of [Bu$_4$N][N$_3$] to **1** which shows two quadrupole doublets corresponding to **2** (81%) and an Fe-based impurity (19%) (Figure S48). An alternative explanation is that the nitrido unit of the anionic [($^{t\mathrm{Bu}}$L)Fe$_3$(μ^3−N)]$^-$ intermediate is highly basic and deprotonates or H-atom abstracts from the solvent or another available H-source to form the neutral imido species ($^{t\mathrm{Bu}}$L)Fe$_3$(μ^3−NH). Given the observed diamagnetism of **2**, the assignment of **2** as the parent imido is unlikely as such assignment would require an odd-electron Fe$^{\mathrm{II}}$/Fe$^{\mathrm{II}}$/Fe$^{\mathrm{I}}$ configuration. Furthermore, no N−H stretch is observed in the IR spectrum (Figure S18) for **2** and the difference map of the SCXRD data (see below) does not show any appreciable e$^-$ density above the nitrido ligand.

The molecular structure of **2** features three Fe ions bridged by a μ^3-nitrido ligand that resides 1.160(7) Å above the [Fe$_3$] plane centroid. Each Fe center adopts a distorted *cis*-divacant octahedral geometry formed by two bridging anilido ligands, a terminally bound di-*tert*-butylphosphine ligand, and the central μ^3-nitrido. Notably, no counterions or protonation of the ligand is apparent, suggesting a net three electron oxidative N-atom transfer reaction has occurred to **1**. Upon N^{3-} atom transfer, expansion of the [Fe$_3$] core is observed as measured by the increase in average Fe−Fe distances from 2.3961[4] Å for **1** to 2.4862[10] Å in **2**. The average Fe−Fe distance of compound **2** is slightly higher than the average Fe−Fe distances of the higher valent nitrido cluster [($^{t\mathrm{bs}}$L)Fe$_3$(μ^3−N)]$^-$ (2.4798[7] Å).[41] The zero-field ^{57}Fe Mössbauer of **2** shows a single major quadrupole doublet (δ, $|\Delta E_Q|$ (mm/s): 0.57, 2.32), and corresponds with the approximate C_3-symmetry observed in the solid-state structure and ^{19}F NMR (Figure S47). Interestingly, the Mössbauer parameters of **2**

https://doi.org/10.1021/jacs.4c07112
J. Am. Chem. Soc. 2024, 146, 25578−25588

Scheme 2. Synthesis of 2 via Multiple Routes

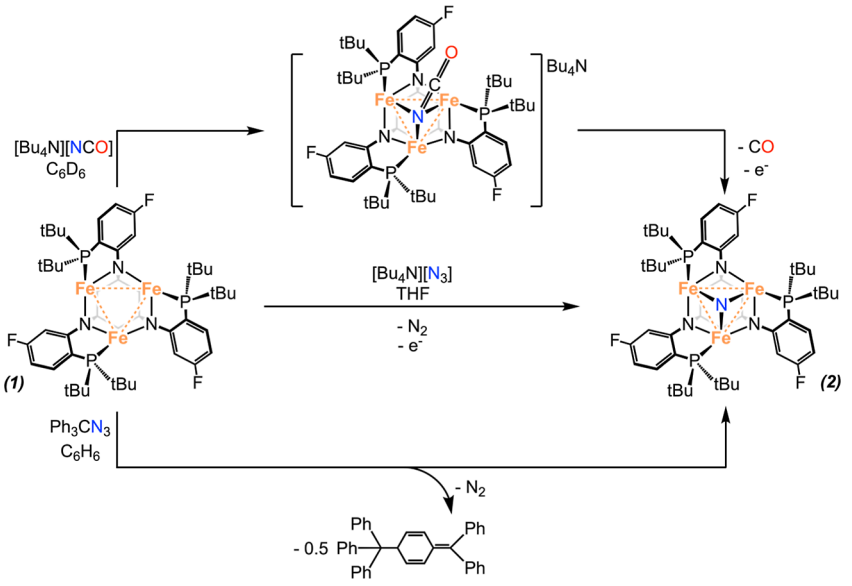

only deviate slightly from the parameters of the all-monovalent parent **1** despite a formal 3-fold oxidation of **1** to **2** and a change in local coordination geometry for each Fe site.

Given the apparent three-electron oxidation of compound **1** to form **2** upon the addition of inorganic azide, we wished to further probe the N-atom extrusion reactivity of **1** with other known N-atom transfer reagents (Scheme 2). The reaction of **1** with tritylazide (Ph_3CN_3) in C_6D_6 results in the immediate formation of **2** and Gomberg's dimer ($Ph_3C(C_6H_5)CPh_2$) as determined by ^{19}F and ^{1}H NMR spectroscopy (Figure S19). The formation of Gomberg's dimer and **2** as opposed to the formally $Fe^{II}/Fe^{II}/Fe^{I}$ trityl imido species ($^{tBu}L)Fe_3(N(CPh_3))$ suggest tritylazide acts a formal three electron oxidant via nitride delivery and $^{\bullet}CPh_3$ generation, lending further support to the assignment of **2** as an all-ferrous nitrido.

Reactions of **1** with tetrabutylammonium cyanate were also probed. Monitoring the reaction of **1** and $[Bu_4N][NCO]$ in C_6D_6 by ^{19}F NMR (Figure S22) showed a new resonance at −66 ppm along with **1** and a low intensity resonance corresponding to **2**. Stirring the reaction for 6 h resulted in an increase concentration of both **2** and the species at −66 ppm (^{19}F NMR) with a corresponding decrease in concentration of **1**. After stirring for 24 h, complete conversion of **1** to **2** was observed. The intermediate resonance observed at −66 ppm (^{19}F NMR) is consistent with the formation of the $[(^{tBu}L)Fe_3(NCO)]^-$ adduct prior to release of CO and the delivery of N^{3-} to the $[Fe_3]$ core. The formation of a $[(^{tBu}L)Fe_3[NCO]]^-$ adduct is further supported by reaction monitoring by IR spectroscopy (Figure S24) which shows an intense stretch at 2199 cm^{-1}. This is notably blueshifted 66 cm^{-1} relative to the $\nu_{NCO}$for $[Bu_4N][NCO]$ which has been previously observed for transition metal cyanate adducts.[58]

Given the ability of **1** to mediate oxidative N^{3-} group transfer chemistry, we were interested in exploring its analogous reactivity with the heavier pnictogens. In particular, discrete late transition metal phosphide complexes have been relatively less explored relative to their lighter nitrido analogues. Addition of a chilled THF solution of the phosphaethynolate reagent[59] $[(dioxane)_{2.5}/(15\text{-crown-5})Na][PCO]$ to a just-thawed THF solution of **1** resulted in a color change from black to dark red upon warming to room temperature. After 30 min of stirring, the ^{19}F NMR spectrum of the crude reaction mixture showed three upfield shifted resonances at −89, −90, and −147 ppm (Figure S27) which correspond to complete conversion of **1** to a new asymmetric product. The wide ^{1}H NMR spectral width of the worked-up product suggest the new asymmetric product is paramagnetic, with >20 broad NMR resonances observable between 40 and −160 ppm (Figure S26). Recrystallization of the crude reaction mixture out of concentrated THF/Et_2O mixtures resulted in black single crystals which were measured by SCXRD and determined to be the Fe_3-phosphido complex, $[(^{tBu}L)Fe_3(\mu^3\text{–}P)(CO)]^-$ (**3**) (Scheme 3).

Scheme 3. Synthesis of 3

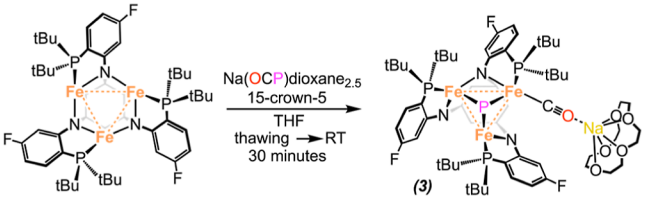

The molecular structure of **3** (Figure 6a) features three distinct Fe centers that are supported by an asymmetrically bound $[^{tBu}L]^{3-}$ ligand scaffold, a (μ^3–P^{3-}) ligand, and a terminally bound carbonyl ligand on one of the Fe sites. The monoanionic $[(^{tBu}L)Fe_3(\mu^3\text{–}P)(CO)]^-$ is charge balanced by a $[Na(15\text{-C-}5)]^+$ cation which is associated with the inner-sphere complex through bonding with the oxygen atom of the carbonyl ligand. Neglecting Fe–Fe bonding interactions, **3** features two, four-coordinate Fe sites (**Fe1** and **Fe2**), and a single, three-coordinate Fe site (**Fe3**). For each of the two four-coordinate Fe sites, the local geometry is best described as distorted tetrahedral. Both **Fe1** and **Fe2** sites feature three common ligand donor atoms: a terminally bound alkyl phosphine (from $[^{tBu}L]^{3-}$), a bridging anilido donor (from $[^{tBu}L]^{3-}$), and the μ^3–P^{3-} capping ligand. The fourth ligand donor, which differentiates the coordination sphere of the **Fe1** and **Fe2** sites, is the terminal carbonyl ligand (for **Fe1**) and a

https://doi.org/10.1021/jacs.4c07112
J. Am. Chem. Soc. 2024, 146, 25578−25588

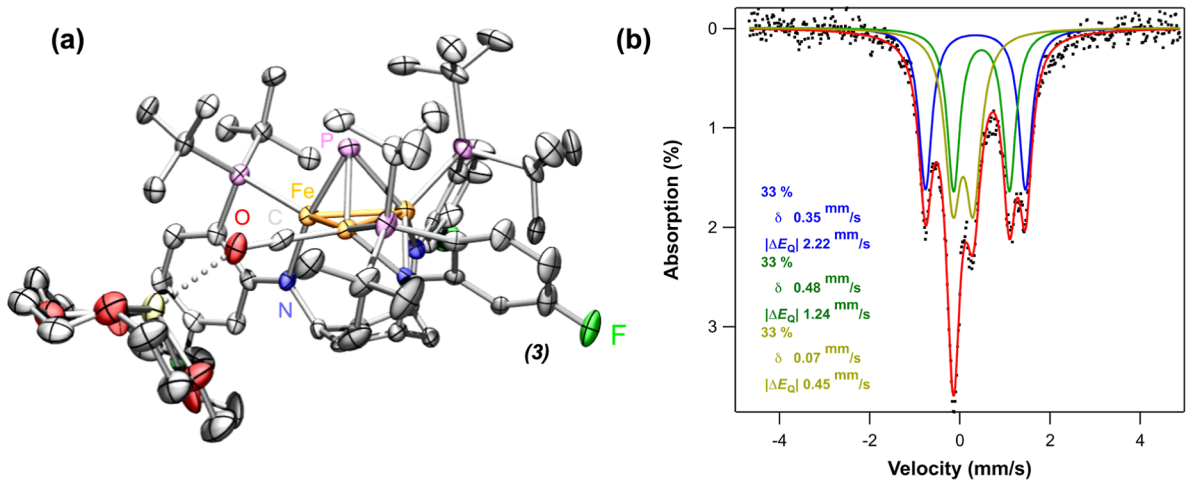

Figure 6. (a) Molecular structure of **3**. Atom colors represent Fe (orange), N (blue), P (pink), F (green), C (gray), O (red), Na (yellow). H atoms omitted for clarity. Structure presented with ellipsoids at 50% probability (b) ^{57}Fe Mössbauer spectrum of **3** (T = 90 K; H = 0 T).

nonbridging anilido donor (from $[^{tBu}L]^{3-}$) (for **Fe2**). For the three coordinate **Fe3** site, the coordination geometry is closest to distorted T-shaped and consists of nonbridging anilido and alkyl phosphine donors (from $[^{tBu}L]^{3-}$) and μ^3−P^{3-} ligand.

The asymmetry of the bound $[^{tBu}L]^{3-}$ ligand of **3** results in significant deviation in the three Fe−Fe distances of 2.3464(10) Å (**Fe1**−**Fe3**), 2.4492(11) Å (**Fe1**−**Fe2**), and 2.5052(11) Å (**Fe2**−**Fe3**). The resulting asymmetry of the [Fe_3] core is further reflected in the zero-field ^{57}Fe Mössbauer spectrum at 90 K where three equally intense features can be resolved [δ, $|\Delta E_Q|$ (mm/s): component 1 (33%) 0.35, *2.22*; component 2 (33%) 0.48, *1.24*; component 3 (33%) 0.07, *0.45*) (Figure 6b)]. The (P^{3-})−[Fe_3(centroid)] distance is 1.7434(14) Å and is over 0.6 Å longer than the corresponding (N^{3-})−[Fe_3(centroid)] distance for **2** of 1.160(7) Å. Correspondingly, the P^{3-} capping ligand is significantly more pyramidalized ($\sum$(∠Fe−$P_{phosphido}$−Fe°) = 197.43[9]° relative the N^{3-} capping ligand of **2** ($\sum$(∠Fe−$N_{nitrido}$−Fe°) = 254[12]°).

The monoanionic nature of **3** is indicative of a mixed-valent [Fe_3] cluster having a formal core oxidation state of $Fe^{II}/Fe^{II}/Fe^{I}$, which is seemingly unstable when the capping pnictides is N^{3-}. The ability to isolate the mixed-valent state for **3** versus **2** could be a combination of the softer μ^3−P^{3-} bridgehead and the presence of the terminally bound carbonyl ligand which can stabilize the cluster via π-backbonding interactions. The IR spectrum of **3** (Figure S28) suggests a significantly reduced CO ligand with an intense C−O stretch being observed at ν = 1743 cm^{-1} and an elongated C−O bond length of 1.194 Å(7) versus 1.13 Å for free CO.

The $\chi_M T$ (300 K) value for compound **3** under a 1 T applied magnetic field was found to be 4.20 emu·K mol^{-1} which is closest to the value expected for a $S = {}^5/_2$ system (4.375 emu K mol^{-1}) (Figure S38). Upon cooling, the $\chi_M T$ value decreases only very slightly until ∼30 K where a steep decline is observed to a minimal 2.005 emu·K mol^{-1} at 2 K. The low temperature decline could be due to ZFS and/or antiferromagnetic coupling interactions between two-three of the Fe ions within the [Fe_3] core of **3**. Like compound **1**, nonsuperposition of the M vs H/T curves of **3** suggest some degree of magnetic anisotropy is present within the [Fe_3] core (Figure S40). The susceptibility and magnetization data were simultaneously fit using eq 1 (see Section 2.2.) assuming a maximum spin $S = {}^5/_2$ ground state. Though reasonable fits were obtained by assuming a giant, single-spin system [g = 1.954, D = −8.848 cm^{-1}, and E = −2.802 cm^{-1} ($|E/D|$ = 0.3167)], it is likely that this assumption is inaccurate given the asymmetry of the [Fe_3] core of **3** and the three different coordination sites of the individual Fe-atoms. Therefore, a more detailed analysis is needed to concretely describe the electronic structure of **3**.

2.5. Electrochemistry of 1−3. The redox capacity of **1**−**3** were explored using cyclic voltammetry (Figure 7). Compounds **1**−**3** exhibit rich electrochemistry, with reversible or quasi-reversible redox events being observed at potentials both anodic and cathodic of the open-circuit potential for each compound. For **1**, scanning cathodically and then anodically from the from the open-circuit potential (OCP: −1.98 V) gives three quasi-reversible redox events at −2.82, −1.87, and −0.70 V (vs Fc/Fc^+). The −2.82 V event is tentatively assigned to a formal one-electron reduction of **1** to the monoanionic $[(^{tBu}L)Fe_3]^-$. The quasi-reversible one electron events at −1.9 and −0.7 V are assigned to the $[(^{tBu}L)Fe_3]^{0/1+}$ and $[(^{tBu}L)Fe_3]^{1+/2+}$ couples, respectively. Scanning oxidatively from the $[(^{tBu}L)Fe_3]^{1+/2+}$ couple, it appears the presumed

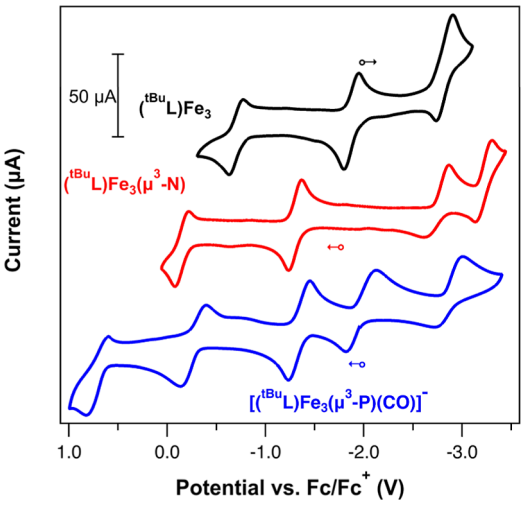

Figure 7. Cyclic voltammograms of **1** (black), **2** (red), and **3** (blue) in THF at 100 mV/s (0.25 M [Bu_4N][PF_6]).

https://doi.org/10.1021/jacs.4c07112
J. Am. Chem. Soc. 2024, 146, 25578−25588

dication $[(^{tBu}L)Fe_3]^{2+}$ is irreversibly oxidized near −0.1 V vs Fc/Fc^+. For **2**, reversible and quasi-reversible oxidations are observed at −1.30 and −0.15 V, respectively. Reductive of the OCP, we first observe a nonreversible reduction event at −2.74 V followed by a quasi-reversible reduction at −3.22 V. The appearance of the first reduction event (relative to $[(^{tBu}L)\text{-}Fe_3(\mu^3\text{–}N)]^0$) at −2.74 V likely indicates that the putative $[(^{tBu}L)Fe(\mu^3\text{–}N)]^-$ intermediate to **2** is highly reducing in THF and thus the inability to isolate this species upon azide (or cyanate) addition is not surprising. For compound **3**, five redox states are observed between 1 and −3.5 V. Scanning anodically from the OCP, a quasi-reversible oxidation event is observed at −2.02 V followed by a reversible event (−1.3 V) and two more quasi-reversible events at −0.27 and +0.71 V. Cathodic of the OCP, a nonreversible reduction event is observed at −2.74 V. The isolation of the oxidation and reduction product(s) of **1**–**3** using appropriate chemical oxidants/reductants are currently underway.

2.6. Single-Molecule Magnetic Behavior of 1 and 3.

Low-valent Fe species in fine-tuned molecular geometries have been shown to exhibit large unquench orbital angular momentum leading to slow magnetic relaxation in the absence of an external magnetic field.[60] Such SMMs have garnered interest in areas of quantum computing, data-storage, and spintronics applications.[61−66] In the realm of transition metal molecular magnetism, high-spin molecular clusters are often targeted for SMMs having ultrahigh magnetic moments for single molecules.[67−70]

Though molecular clusters and low-valent mononuclear Fe compounds have been thoroughly studied in the area of molecular magnetism, molecular clusters featuring one or more low-valent Fe^I ion have been much less studied in this regard. Of the reported transition metal-based SMMs formally containing one or more low valent Fe^I ion(s), our group previously reported the $Fe^{II}/Fe^{II}/Fe^I$ compound $[(^{tbs}L)Fe_3]^-$[51] which represents a rare example of a low valent Fe-cluster SMM having an energy barrier to spin reorientation of U = 22.6(2) cm^{-1}.[51]

With the low-valent compounds **1** and **3** in hand, we wished to explore their SMM properties using alternating current (ac) SQUID magnetometry in the absence of an applied magnetic field. At 1.8 K, the out-of-phase component (χ_M'') of the ac magnetic susceptibility versus frequency plot for the all monovalent **1** shows a tail of a χ_M'' signal that increases in magnitude outside of the 1000 Hz frequency limit (Figure S36). The appearance of a χ_M'' signal in the absence of an external magnetic field suggest the presence of slow magnetic relaxation. However, the lack of a discernible signal maximum within the 1−1000 Hz frequency range suggest magnetic relaxation times less than ∼0.16 ms and precludes further analysis of the magnetization dynamics to be made.

For the formally $[Fe^{II}/Fe^{II}/Fe^I]$ cluster **3**, a χ_M'' signal with a well-defined maximum ∼100 Hz at 1.8 K (H = 0 T) is observed (Figure 8a). Increasing the temperature from 1.8 K, the χ_M'' signal decreases in magnitude but remains at stationary frequency until T = 2.6 K where the signal maximum moves quickly to higher frequencies and outside of the upper limit frequency range at 4.0 K. Using the ac susceptibility data, Cole−Cole plots (χ_M'' vs χ_M') (Figure S44) were constructed and fit with the generalized Debye Equation (eq S1). This procedure allowed the extraction of the magnetic relaxation times at each temperature which were subsequently used to construct an Arrhenius plot ($\ln(\tau)$ vs $1/T$) (Figure 8b). In the

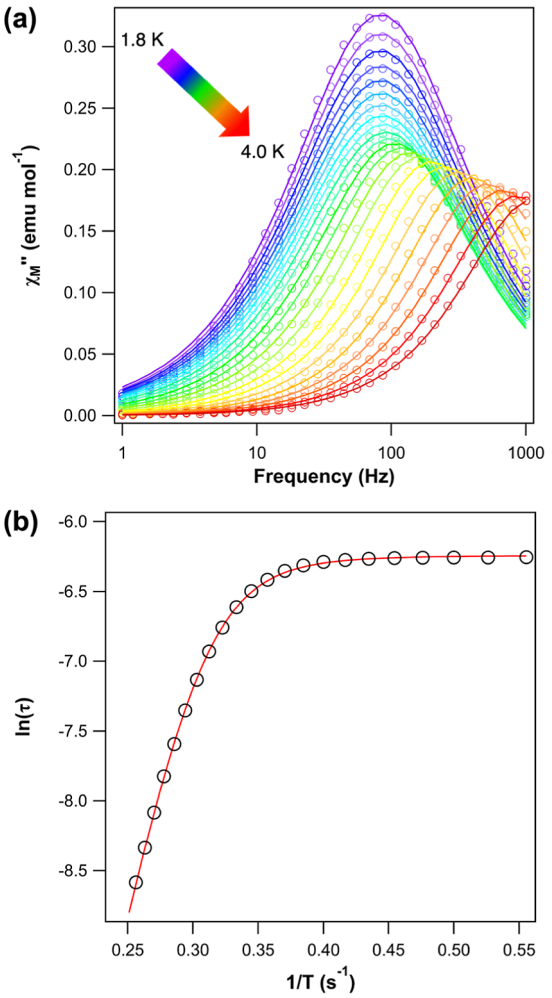

Figure 8. (a) The temperature dependence of the molar out-of-phase component (χ_M'') of the alternating current (ac) magnetic susceptibility of **3** (T = 1.8−4 K; H = 0 T). (**b**) Arrhenius plot of **3**. The line represents the fit to the spin relaxation times (open circles) of **3** using eq 2.

high temperature regime (T = 3.6−4 K), the linearity of $\ln(\tau)$ versus inverse temperature suggests an exponential temperature dependence of τ and indicates the spin relaxation in this temperature range is likely dominated by an Orbach mechanism.[71] At intermediate temperatures (T = 3.6−2.5 K), the deviation from linearity of the $\ln(\tau)$ vs $1/T$ plot suggests an increased contribution of spin relaxation by other mechanisms such as spin−lattice mediated Raman and/or temperature independent quantum tunneling processes. Notably, the relaxation times within the lowest temperature regime (T = 2.5−1.8 K) are nearly temperature independent and indicate quantum tunneling of the magnetization is likely the dominate spin relaxation mechanism at these temperatures.

The Arrhenius plot was fit using eq 2 which includes the spin relaxation through Orbach, Raman, and quantum tunneling processes

$$\tau^{-1} = {\tau_{QTM}}^{-1} + CT^n + {\tau_0}^{-1} \exp\left(-\frac{U}{k_bT}\right) \quad (2)$$

This fitting procedure resulted in values for the Arrhenius parameters of ${\tau_{QTM}}^{-1}$ = 514(4) s^{-1}, C = 0.014(3), n = 8, τ_0 = 2.9(5) × 10^{-9} s, and U = 30.7(6) cm^{-1}. Though modest, the value of the energy barrier to spin relaxation reversal of U =

https://doi.org/10.1021/jacs.4c07112
J. Am. Chem. Soc. 2024, 146, 25578−25588

30.7(6) cm^{-1} for **3** is notably higher than the energy barrier for the previously reported $Fe^{II}/Fe^{II}/Fe^{I}$ species $[(^{tbs}L)Fe_3]^-$ (U = 22.6(2) cm^{-1}). For $[(^{tbs}L)Fe_3]^-$, the origin of the magnetic anisotropy is predicted to originate from strong direct and double exchange interactions which gives rise to an overall $S = {}^{11}/_2$ high spin ground state for $[(^{tbs}L)Fe_3]^-$. For **3**, the maximum $\chi_M T$ value at any temperature falls well short from the expected value of 17.875 emu mol^{-1} for a ferromagnetically coupled high-spin $Fe^{II}/Fe^{II}/Fe^{I}$ core. Thus, it is likely that the mechanism of spin relaxation for **3** differs significantly from that of $[(^{tbs}L)Fe_3]^-$. This hypothesis is further supported by analysis of the in-phase component of the ac magnetic susceptibility of **3** which shows that the asymptotic decline of the χ_M' signal fails to approach 0 emu mol^{-1} at any temperature measured (Figure S43) suggesting that a significant portion of the magnetic moment of **3** does not undergo slow magnetic relaxation. One explanation for this observation is that only moderate to weak magnetic communication between the individual Fe sites of **3** is apparent and not all the Fe sites exhibit slow magnetic relaxation. To this end, further spectroscopic and computational studies will be needed to fully explain to the origin of the SMM behavior in **3**.

3. CONCLUSION

This study describes a new trianionic anilidophosphine ligand platform $[^{tBu}L]^{3-}$ that is used to stabilize the all-Fe^{I} trinuclear cluster $(^{tBu}L)Fe_3$ (**1**). Compound **1** features very close Fe−Fe distances between formally Fe^{I} ions which results in an overall $S = {}^9/_2$ spin ground state being observed. The polynuclear nature of **1** facilitates multielectron reduction of azides and cyanates to give the neutral all ferrous Fe-nitrido species $(^{tBu}L)Fe_3(\mu^3{-}N)$ (**2**). The oxidative atom transfer chemistry of **1** was expanded to the heavier pnictides and includes the two electron reduction of $[OCP]^-$ to give the unique mixed-valent $Fe^{II}/Fe^{II}/Fe^{I}$ phosphido complex $[(^{tBu}L)Fe_3(\mu^3{-}P)(CO)]^-$. The formally low-valent **1** and **3** exhibit slow spin relaxation dynamics in the absence of an external magnetic field. While a magnetization energy barrier could not be obtained for **1**, a value of U = 30.7(6) cm^{-1} was obtained for **3**. The faster spin relaxation dynamics of **1** relative to **3** is not surprising given the smaller value of $D = -2.2$ cm^{-1} for **1** (vs $D = -8.848$ cm^{-1} for **3**), which indicates small energy splitting between the magnetic sublevels. The foregoing study showcases a polynuclear Fe^{I} system that mediates intramolecular redox chemistry between multiple Fe^{I} ions and exemplifies the redox flexibility latent in the midvalent oxidation products. While the chemistry reported herein draw strong inspiration from early polycarbonyl cluster chemistry to support pnictide cluster formation,[17,21,23−28] templated clusters offer the distinct advantage of crafting the metal primary coordination sphere to facilitate cooperative substrate activation without compromising the cluster core integrity. Studies involving the reactivity of compound **1** with environmentally relevant small molecules such as N_2, CO, and CO_2 are currently underway.

■ ASSOCIATED CONTENT

Supporting Information

The Supporting Information is available free of charge at https://pubs.acs.org/doi/10.1021/jacs.4c07112.

Materials and methods, synthetic procedures, multinuclear NMR spectra, IR spectra, ^{57}Fe Mössbauer spectra, magnetometry data, and XRD refine details/solid state structures (PDF)

Accession Codes

CCDC 2352501−2352503 contain the supplementary crystallographic data for this paper. These data can be obtained free of charge via www.ccdc.cam.ac.uk/data_request/cif, or by emailing data_request@ccdc.cam.ac.uk, or by contacting The Cambridge Crystallographic Data Centre, 12 Union Road, Cambridge CB2 1EZ, UK; fax: +44 1223 336033.

■ AUTHOR INFORMATION

Corresponding Author

Theodore A. Betley − *Department of Chemistry and Chemical Biology, Harvard University, Cambridge, Massachusetts 02138, United States;* orcid.org/0000-0001-5946-9629; Email: betley@chemistry.harvard.edu

Authors

Trevor P. Latendresse − *Department of Chemistry and Chemical Biology, Harvard University, Cambridge, Massachusetts 02138, United States*

Nicholas P. Litak − *Department of Chemistry and Chemical Biology, Harvard University, Cambridge, Massachusetts 02138, United States*

Joy S. Zeng − *Department of Chemistry and Chemical Biology, Harvard University, Cambridge, Massachusetts 02138, United States;* orcid.org/0000-0002-3443-3504

Shao-Liang Zheng − *Department of Chemistry and Chemical Biology, Harvard University, Cambridge, Massachusetts 02138, United States;* orcid.org/0000-0002-6432-9943

Complete contact information is available at: https://pubs.acs.org/10.1021/jacs.4c07112

Notes

The authors declare no competing financial interest.

■ ACKNOWLEDGMENTS

T.P.L. acknowledges the generous support of National Institutes of Health through a Ruth L. Kirschstein Postdoctoral Fellowship (1F32GM145088-01A1). T.A.B. acknowledges the generous support of the NIH (GM145752), and NSF (CHE-2247817). We acknowledge support from the Major Research Instrumentation (MRI) Program of the National Science Foundation under NSF award no. 2216066 for the X-ray facility.

■ REFERENCES

(1) Chalkley, M. J.; Drover, M. W.; Peters, J. C. Catalytic N_2-to-NH_3(or -N_2H_4) conversion by well-defined molecular coordination complexes. *Chem. Rev.* **2020**, *120*, 5582−5636.

(2) Chatt, J.; Dilworth, J. R.; Richards, R. L. Recent advances in the chemistry of nitrogen fixation. *Chem. Rev.* **1978**, *78*, 589−625.

(3) Allen, A. D.; Harris, R. O.; Loescher, B.; Stevens, J. R.; Whiteley, R. N. Dinitrogen complexes of the transition metals. *Chem. Rev.* **1973**, *73*, 11−20.

(4) Boutin, E.; Merakeb, L.; Ma, B.; Boudy, B.; Wang, M.; Bonin, J.; Anxolabéhère-Mallart, E.; Robert, M. Molecular catalysis of CO_2 reduction: recent advances and perspectives in electrochemical and light-driven processes with selected Fe, Ni and Co aza macrocyclic and polypyridine complexes. *Chem. Soc. Rev.* **2020**, *49*, 5772−5809.

(5) Aresta, M.; Dibenedetto, A.; Angelini, A. Catalysis for the valorization of exhaust carbon: from CO_2 to chemicals, materials, and fuels. technological use of CO_2. *Chem. Rev.* **2014**, *114*, 1709−1742.

(6) Appel, A. M.; Bercaw, J. E.; Bocarsly, A. B.; Dobbek, H.; DuBois, D. L.; Dupuis, M.; Ferry, J. G.; Fujita, E.; Hille, R.; Kenis, P. J. A.; Kerfeld, C. A.; Morris, R. H.; Peden, C. H. F.; Portis, A. R.; Ragsdale, S. W.; Rauchfuss, T. B.; Reek, J. N. H.; Seefeldt, L. C.; Thauer, R. K.; Waldrop, G. L. Frontiers, opportunities, and challenges in biochemical and chemical catalysis of CO_2 fixation. *Chem. Rev.* **2013**, *113*, 6621−6658.
(7) Carboni, M.; Latour, J. M. Enzymes with an heterodinuclear iron-manganese active site: Curiosity or necessity? *Coord. Chem. Rev.* **2011**, *255*, 186−202.
(8) Dos Santos, P. C.; Igarashi, R. Y.; Lee, H. I.; Hoffman, B. M.; Seefeldt, L. C.; Dean, D. R. Substrate interactions with the nitrogenase active site. *Acc. Chem. Res.* **2005**, *38*, 208−214.
(9) Burgess, B. K.; Lowe, D. J. Mechanism of molybdenum nitrogenase. *Chem. Rev.* **1996**, *96*, 2983−3012.
(10) Ma, Z.; Zaera, F. Heterogeneous catalysis by metals. In *Encyclopedia of Inorganic Chemistry*; John Wiley & Sons, Ltd, 2006.
(11) Dong, Y.; Lipschutz, M. I.; Witzke, R. J.; Panetier, J. A.; Tilley, T. D. Switchable Product Selectivity in Diazoalkane Coupling Catalyzed by a Two-Coordinate Cobalt Complex. *ACS Catal.* **2021**, *11*, 11160−11170.
(12) Reiners, M.; Baabe, D.; Münster, K.; Zaretzke, M. K.; Freytag, M.; Jones, P. G.; Coppel, Y.; Bontemps, S.; Rosal, I. D.; Maron, L.; Walter, M. D. NH_3 formation from N_2 and H_2 mediated by molecular tri-iron complexes. *Nat. Chem.* **2020**, *12*, 740−746.
(13) Lee, Y.; Sloane, F. T.; Blondin, G.; Abboud, K. A.; García-Serres, R.; Murray, L. J. Dinitrogen activation upon reduction of a triiron (II) complex. *Angew. Chem., Int. Ed.* **2015**, *54*, 1499−1503.
(14) McWilliams, S. F.; Holland, P. L. Dinitrogen binding and cleavage by multinuclear iron complexes. *Acc. Chem. Res.* **2015**, *48*, 2059−2065.
(15) Anderson, J. S.; Rittle, J.; Peters, J. C. Catalytic conversion of nitrogen to ammonia by an iron model complex. *Nature* **2013**, *501*, 84−87.
(16) Rodriguez, M. M.; Bill, E.; Brennessel, W. W.; Holland, P. L. N_2 reduction and hydrogenation to ammonia by a molecular iron-potassium complex. *Science* **2011**, *334*, 780−783.
(17) Mehn, M. P.; Peters, J. C. Mid-to-high-valent imido and nitrido complexes of iron. *J. Inorg. Biochem.* **2006**, *100*, 634−643.
(18) Bennett, M. V.; Stoian, S.; Bominaar, E. L.; Münck, E.; Holm, R. H. Initial members of the family of molecular mid-valent high-nuclearlrity iron nitrides: $[Fe_4N_2X_{10}]^{4-}$ and $[Fe_{10}N_8X_{12}]^{5-}$ (X = Cl^-, Br^-). *J. Am. Chem. Soc.* **2005**, *127*, 12378−12386.
(19) Brown, S. D.; Betley, T. A.; Peters, J. C. A Low-Spin d^5 Iron Imide: Nitrene Capture by Low-Coordinate Iron(I) Provides the 4-Coordinate Fe(III) Complex $[PhB(CH_2PPh_2)_3]Fe$ = N-p-tolyl. *J. Am. Chem. Soc.* **2003**, *125*, 322−323.
(20) Betley, T. A.; Peters, J. C. Dinitrogen chemistry from trigonally coordinated iron and cobalt platforms. *J. Am. Chem. Soc.* **2003**, *125*, 10782−10783.
(21) *Unusual Structures and Physical Properties in Organometallic Chemistry*; Gielen, M., Willem, R., Wrackmeyer, B., Eds.; John Wiley & Sons, 2003.
(22) Jenkins, D. M.; Betley, T. A.; Peters, J. C. Oxidative group transfer to Co(I) affords a terminal Co(III) imido complex. *J. Am. Chem. Soc.* **2002**, *124*, 11238−11239.
(23) Whitmire, K. H. Main Group-Transition Metal Cluster Compounds of the Group 15 Elements. *Advances in Organometallic Chemistry*; Academic Press, 1998; Vol. *42*, pp 2−146.
(24) Koide, Y.; Bautista, M. T.; White, P. S.; Schauer, C. K. Fe_3-Triangle opening and closing by a single two-electron process in the bicapped triiron clusters $Fe_3(CO)_9(\mu_3\text{-}PML_n)_2$ (ML_n = $CpFe(CO)_2$, $CpMn(CO)_2$). *Inorg. Chem.* **1992**, *31*, 3690−3692.
(25) Huttner, G.; Knoll, K. R. RP-Bridged Metal Carbonyl Clusters: Synthesis, Properties, and Reactions. *Angew. Chem., Int. Ed.* **1987**, *26*, 743−760.
(26) Lang, H.; Huttner, G.; Zsolnai, L.; Mohr, G.; Sigwarth, B.; Weber, U.; Orama, O.; Jibril, I. Diphosphor, phosphor-arsen- und antimonatome als clusterbaugruppen. *J. Organomet. Chem.* **1986**, *304*, 157−179.
(27) Whitmire, K. H.; Lagrone, C. B.; Churchill, M. R.; Fettinger, J. C.; Biondi, L. V. Synthesis and characterization of an iron carbonyl cluster containing bismuth: crystal and molecular structure of tetraethylammonium (μ^3-bismuthido) nonacarbonyl (μ^3-carbonyl)-triangulo-triferrate (1-), $[Et_4N]$ $[(\mu^3\text{-}Bi)Fe_3(CO)_9(\mu^3\text{-}CO)]$, a closo cluster of the first transition series with a large heteroatom. *Inorg. Chem.* **1984**, *23*, 4227−4232.
(28) Fjare, D. E.; Gladfelter, W. L. Synthesis and characterization of a nitrosyl, a nitrido, and an imido carbonyl cluster. *J. Am. Chem. Soc.* **1981**, *103*, 1572−1574.
(29) Mokhtarzadeh, C. C.; Moore, C. E.; Rheingold, A. L.; Figueroa, J. S. Terminal Iron Carbyne Complexes Derived from Arrested CO_2 Reductive Disproportionation. *Angew. Chem.* **2017**, *129*, 11034−11039.
(30) Agnew, D. W.; Sampson, M. D.; Moore, C. E.; Rheingold, A. L.; Kubiak, C. P.; Figueroa, J. S. Electrochemical properties and CO_2-reduction ability of m-terphenyl isocyanide supported manganese tricarbonyl complexes. *Inorg. Chem.* **2016**, *55*, 12400−12408.
(31) Maher, J. M.; Cooper, N. J. Reduction of carbon dioxide to carbon monoxide by transition-metal dianions. *J. Am. Chem. Soc.* **1980**, *102*, 7604−7606.
(32) Deegan, M. M.; Peters, J. C. O-Functionalization of a cobalt carbonyl generates a terminal cobalt carbyne. *Chem. Commun.* **2019**, *55*, 9531−9534.
(33) Suess, D. L.; Peters, J. C. A CO-derived iron dicarbyne that releases olefin upon hydrogenation. *J. Am. Chem. Soc.* **2013**, *135*, 12580−12583.
(34) Carnahan, E. M.; Protasiewicz, J. D.; Lippard, S. J. The 15 years of reductive coupling: what have we learned? *Acc. Chem. Res.* **1993**, *26*, 90−97.
(35) Beamer, A. W.; Buss, J. A. Synthesis, structural characterization, and CO_2 reactivity of a constitutionally analogous series of tricopper mono-di-and trihydrides. *J. Am. Chem. Soc.* **2023**, *145*, 12911−12919.
(36) Arnett, C. H.; Agapie, T. Activation of an open shell, carbyne-bridged diiron complex toward binding of dinitrogen. *J. Am. Chem. Soc.* **2020**, *142*, 10059−10068.
(37) Liu, T.; Gau, M. R.; Tomson, N. C. Mimicking the constrained geometry of a nitrogen-fixation intermediate. *J. Am. Chem. Soc.* **2020**, *142*, 8142−8146.
(38) McSkimming, A.; Sridharan, A.; Thompson, N. B.; Müller, P.; Suess, D. L. An $[Fe_4S_4]^{3+}$-alkyl cluster stabilized by an expanded scorpionate ligand. *J. Am. Chem. Soc.* **2020**, *142*, 14314−14323.
(39) McSkimming, A.; Suess, D. L. Selective synthesis of site-differentiated Fe_4S_4 and Fe_6S_6 clusters. *Inorg. Chem.* **2018**, *57*, 14904−14912.
(40) Arnett, C. H.; Chalkley, M. J.; Agapie, T. A thermodynamic model for redox-dependent binding of carbon monoxide at site-differentiated, high spin iron clusters. *J. Am. Chem. Soc.* **2018**, *140*, 5569−5578.
(41) Creutz, S. E.; Peters, J. C. Diiron bridged-thiolate complexes that bind N_2 at the $Fe^{II}Fe^{II}$, $Fe^{II}Fe^{I}$, and $Fe^{I}Fe^{I}$ redox states. *J. Am. Chem. Soc.* **2015**, *137*, 7310−7313.
(42) Guillet, G. L.; Sloane, F. T.; Ermert, D. M.; Calkins, M. W.; Peprah, M. K.; Knowles, E. S.; Čižmár, E.; Abboud, K. A.; Meisel, M. W.; Murray, L. J. Preorganized assembly of three iron(ii) or manganese(ii) β-diketiminate complexes using a cyclophane ligand. *Chem. Commun.* **2013**, *49*, 6635.
(43) Zhao, Q.; Betley, T. A. Synthesis and redox properties of triiron complexes featuring strong Fe-Fe interactions. *Angew. Chem., Int. Ed.* **2011**, *50*, 709−712.
(44) Stack, T. D. P.; Holm, R. H. Subsite-differentiated analogs of biological $[4Fe\text{-}4S]^{2+}$ clusters: synthesis, solution and solid-state structures, and subsite-specific reactions. *J. Am. Chem. Soc.* **1988**, *110*, 2484−2494.
(45) Powers, T. M.; Fout, A. R.; Zheng, S. L.; Betley, T. A. Oxidative group transfer to a triiron complex to form a nucleophilic μ^3-nitride, $[Fe_3(\mu^3\text{-}N)]^-$. *J. Am. Chem. Soc.* **2011**, *133*, 3336−3338.

https://doi.org/10.1021/jacs.4c07112
J. Am. Chem. Soc. 2024, 146, 25578−25588

(46) Powers, T. M.; Betley, T. A. Testing the polynuclear hypothesis: Multielectron reduction of small molecules by triiron reaction sites. *J. Am. Chem. Soc.* **2013**, *135*, 12289−12296.
(47) Tolman, C. A. Steric effects of phosphorus ligands in organometallic chemistry and homogeneous catalysis. *Chem. Rev.* **1977**, *77*, 313−348.
(48) Witzke, R. J.; Hait, D.; Head-Gordon, M.; Tilley, T. D. Two-coordinate iron(I) complexes on the edge of stability: influence of dispersion and steric effects. *Organometallics* **2021**, *40*, 1758−1764.
(49) Zadrozny, J. M.; Xiao, D. J.; Atanasov, M.; Long, G. J.; Grandjean, F.; Neese, F.; Long, J. R. Magnetic blocking in a linear iron(I) complex. *Nat. Chem.* **2013**, *5*, 577−581.
(50) Shannon, R. D. Revised effective ionic radii and systematic studies of interatomic distances in halides and chalcogenides. *Acta Crystallogr., Sect. A: Cryst. Phys., Diffr., Theor. Gen. Crystallogr.* **1976**, *32*, 751−767.
(51) Hernández Sánchez, R.; Bartholomew, A. K.; Powers, T. M.; Ménard, G.; Betley, T. A. Maximizing electron exchange in a $[Fe_3]$ cluster. *J. Am. Chem. Soc.* **2016**, *138*, 2235−2243.
(52) Chilton, N. F.; Anderson, R. P.; Turner, L. D.; Soncini, A.; Murray, K. S. PHI: A powerful new program for the analysis of anisotropic monomeric and exchange-coupled polynuclear *d*- and *f*-block complexes. *J. Comput. Chem.* **2013**, *34*, 1164−1175.
(53) Neese, F. Software update: The ORCA program system—Version 5.0. *Wiley Interdiscip. Rev.: Comput. Mol. Sci.* **2022**, *12* (5), No. e1606.
(54) Tao, J.; Perdew, J. P.; Staroverov, V. N.; Scuseria, G. E. Climbing the Density Functional Ladder: Nonempirical Meta-Generalized Gradient Approximation Designed for Molecules and Solids. *Phys. Rev. Lett.* **2003**, *91*, 146401.
(55) Staroverov, V. N.; Scuseria, G. E.; Tao, J.; Perdew, J. P. Comparative assessment of a new nonempirical density functional: Molecules and hydrogen-bonded complexes. *J. Chem. Phys.* **2003**, *119*, 12129−12137.
(56) Weigend, F.; Ahlrichs, R. Balanced basis sets of split valence, triple zeta valence and quadruple zeta valence quality for H to Rn: Design and assessment of accuracy. *Phys. Chem. Chem. Phys.* **2005**, *7*, 3297.
(57) Pantazis, D. A.; Chen, X.-Y.; Landis, C. R.; Neese, F. All-Electron Scalar Relativistic Basis Sets for Third-Row Transition Metal Atoms. *J. Chem. Theory Comput.* **2008**, *4*, 908−919.
(58) Silvia, J. S.; Cummins, C. C. Two-electron reduction of a vanadium (V) nitride by CO to release cyanate and open a coordination site. *J. Am. Chem. Soc.* **2009**, *131*, 446−447.
(59) Heift, D.; Benkő, Z.; Grützmacher, H. Coulomb repulsion versus cycloaddition: formation of anionic four-membered rings from sodium phosphaethynolate Na (OCP). *Dalton Trans.* **2014**, *43*, 831−840.
(60) Khurana, R.; Ali, M. E. Single-molecule magnetism in linear Fe(I) complexes with aufbau and non-aufbau ground states. *Inorg. Chem.* **2022**, *61*, 15335−15345.
(61) Bayliss, S. L.; Laorenza, D. W.; Mintun, P. J.; Kovos, B. D.; Freedman, D. E.; Awschalom, D. D. Optically addressable molecular spins for quantum information processing. *Science* **2020**, *370*, 1309−1312.
(62) Hymas, K.; Soncini, A. Molecular spintronics using single-molecule magnets under irradiation. *Phys. Rev. B* **2019**, *99*, 245404.
(63) Gaita-Ariño, A.; Luis, F.; Hill, S.; Coronado, E. Molecular spins for quantum computation. *Nat. Chem.* **2019**, *11*, 301−309.
(64) Mannini, M.; Pineider, F.; Danieli, C.; Totti, F.; Sorace, L.; Sainctavit, P.; Arrio, M. A.; Otero, E.; Joly, L.; Cezar, J. C.; Cornia, A.; Sessoli, R. Quantum tunnelling of the magnetization in a monolayer of oriented single-molecule magnets. *Nature* **2010**, *468*, 417−421.
(65) Mannini, M.; Pineider, F.; Sainctavit, P.; Danieli, C.; Otero, E.; Sciancalepore, C.; Talarico, A. M.; Arrio, M. A.; Cornia, A.; Gatteschi, D.; Sessoli, R. Magnetic memory of a single-molecule quantum magnet wired to a gold surface. *Nat. Mater.* **2009**, *8*, 194−197.
(66) Affronte, M.; Troiani, F.; Ghirri, A.; Candini, A.; Evangelisti, M.; Corradini, V.; Carretta, S.; Santini, P.; Amoretti, G.; Tuna, F.; Timco, G.; Winpenny, R. E. P. Single-molecule magnets for quantum computation. *J. Phys. D: Appl. Phys.* **2007**, *40*, 2999−3004.
(67) Abbasi, P.; Quinn, K.; Alexandropoulos, D. I.; Damjanović, M.; Wernsdorfer, W.; Escuer, A.; Mayans, J.; Pilkington, M.; Stamatatos, T. C. Transition metal single-molecule magnets: a $\{Mn_{31}\}$ nanosized cluster with a large energy barrier of ∼60 K and magnetic hysteresis at ∼ 5 K. *J. Am. Chem. Soc.* **2017**, *139*, 15644−15647.
(68) Murugesu, M.; Takahashi, S.; Wilson, A.; Abboud, K. A.; Wernsdorfer, W.; Hill, S.; Christou, G. Large Mn_{25} single-molecule magnet with spin $S = {}^{51}/_{2}$: magnetic and high-frequency electron paramagnetic resonance spectroscopic characterization of a giant spin state. *Inorg. Chem.* **2008**, *47*, 9459−9470.
(69) Gatteschi, D.; Sessoli, R.; Villain, J. *Molecular Nanomagnets*; Oxford University Press, 2006.
(70) Sessoli, R.; Gatteschi, D.; Caneschi, A.; Novak, M. A. Magnetic bistability in a metal-ion cluster. *Nature* **1993**, *365*, 141−143.
(71) Liddle, S. T.; van Slageren, J. Improving f-element single-molecule magnets. *Chem. Soc. Rev.* **2015**, *44*, 6655−6669.

https://doi.org/10.1021/jacs.4c07112
J. Am. Chem. Soc. 2024, 146, 25578−25588